Carbohydrate Polymers 92 (2013) 69–76

Contents lists available at SciVerse ScienceDirect

Carbohydrate Polymers

journal homepage: www.elsevier.com/locate/carbpol

Preparation and properties of carboxylated styrene-butadiene rubber/cellulose nanocrystals composites

Xiaodong Cao [a], Chuanhui Xu [a], Yuhong Liu [a], Yukun Chen [b,c,*]

[a] School of Materials Science and Engineering, South China University of Technology, Guangzhou 510640, China
[b] The Key Laboratory of Polymer Processing Engineering, Ministry of Education, China (South China University of Technology), Guangzhou 510640, China
[c] School of Mechanical and Automotive Engineering, South China University of Technology, Guangzhou 510640, China

ARTICLE INFO

Article history:
Received 19 July 2012
Received in revised form 29 August 2012
Accepted 24 September 2012
Available online 3 October 2012

Keywords:
Composites
Cellulose nanocrystals
Carboxylated styrene-butadiene rubber
Properties

ABSTRACT

A series of carboxylated styrene-butadiene rubber (XSBR)/cellulose nanocrystals (CNs) latex composites were successfully prepared. The vulcanization process, morphology, dynamic viscoelastic behavior, dynamic mechanical property, thermal and mechanical performance of the XSBR/CNs composites were investigated in detail. The results revealed that CNs were dispersed uniformly in the XSBR matrix and formed a strong filler–filler network. The dynamic mechanical analysis (DMA) showed that the glass transition temperature (T_g) of XSBR matrix was shifted from 48.45 to 50.64 °C with 3 phr CNs, but decreased from 50.64 to 46.28 °C when further increasing CNs content up to 15 phr. The composites exhibited a significant enhancement in tensile strength (from 16.9 to 24.1 MPa) and tear strength (from 43.5 to 65.2 MPa) with loading CNs from 0 to 15 phr. In addition, the thermo-gravimetric analysis (TGA) showed that the temperature at 5% weight loss of the XSBR/CNs composites decreased slightly with an increase of the CNs content.

1. Introduction

In general, most of rubbers were reinforced with various fillers for their industry applications. Up to date, various reinforcing agents, such as clay (Kim, Seo, & Jeong, 2003; Kuan, Ma, Chuang, & Su, 2005; Lee & Lin, 2006; Lee, Hwang, & Liu, 2006), multiwall carbon nanotubes (Bokobza, Rahmani, Belin, Bruneel, & El Bounia, 2008; Kuan, Ma, Chang, Yuen, et al., 2005; Kwon & Kim, 2005), carbon black (Dupres, Long, Albouy, & Sotta, 2009) and silica (Thongsang, Sombatsompop, & Ansarifar, 2008), have being used to enhance the mechanical and abrasion properties of cured rubbers. However, they are more or less charged with using the depleting petroleum resources or natural gas for their manufacture, directly or indirectly causing an increase in the carbon footprint and contributing to the accumulation of green house gases. Therefore, with the gradual drying up of petroleum and the higher demand of environmental protection, reinforcements from bio-based renewable resources are receiving increased attention in the scientific community. Tremendous efforts were focused on the development of new materials as viable alternatives that could replace conventional reinforcements in the rubber industry.

Polysaccharides have been used for a wide range of applications such as food, packaging, agricultural chemicals, and biomedical devices. Starch, as one of the most promising biodegradable materials, has been creatively used as reinforcing filler in rubbers to lower the rolling resistance and reduce the use of carbon black amount (Wu, Qi, Liang, & Zhang, 2006). Cellulose, as a most abundant biorenewable material in the world, has being utilized extensively as textile fibers, chemical precursors and food additives etc. In recent years, there has been an increased application of cellulose nanocrystals (CNs) as the load-bearing constituent in the development of new and inexpensive polymer nanocomposite materials (Helbert, Cavaille, & Dufresne, 1996; Sturcova, Davies, & Eichhorn, 2005). As compared to other inorganic reinforcing fillers, CNs have many additional advantages, including positive ecological, wide variety of fillers available throughout the world, low density, low energy consumption in manufacturing, ease for recycling by combustion, high sound attenuation, and comparatively easy processability due to their nonabrasive nature, which allows high filling levels, in turn resulting significant cost savings (Azizi Samir, Alloin, & Dufresne, 2005; Podsiadlo et al., 2005). Since the first announcement of using cellulose nanocrystals from tunicin (an animal cellulose) as a reinforcing phase in a matrix of latex by Favier, Chanzy, and Cavaille (1995) the use of CNs from various sources such as cotton (Fengel & Wegner, 1984), tunicate (Mathew & Dufresne, 2002; Terech, Chazeau, & Cavaille, 1999), algae (Revol, 1982; Hanley, Giasson, Revol, & Gray, 1992), bacteria (Grunert & Winter, 2002; Tokoh, Takabe, Fujita, & Saiki, 1998), ramie (Lu,

* Corresponding author at: School of Mechanical and Automotive Engineering, South China University of Technology, Guangzhou 510640, China.
Tel.: +86 20 87110804; fax: +86 20 85293483.
E-mail address: cyk@scut.edu.cn (Y. Chen).

0144-8617/$ – see front matter. Crown Copyright © 2012 Published by Elsevier Ltd. All rights reserved.
http://dx.doi.org/10.1016/j.carbpol.2012.09.054

Weng, & Cao, 2006) and wood (Araki, Wada, Kuga, & Okano, 1998; Beck-Candanedo, Roman, & Gray, 2005), for the preparation of high performance composite materials based on a wide range of polymers matrices have been investigated widely (Cao, Habibi, & Lucia, 2009; Cao, Habibi, Magalhaes, Rojas, & Lucia, 2011; Chen, Liu, Chang, Cao, & Anderson, 2009; Magalhaes, Cao, & Lucia, 2009). To the best of our knowledge, however, research on CNs as filler for reinforcing of rubber can hardly be found in the literatures (Bai & Li, 2009; Bendahou, Kaddami, & Dufresne, 2010; Xu, Gu, Luo, & Jia, 2012).

Carboxylated styrene-butadiene rubber (XSBR) is a copolymer of styrene, butadiene and a small amount of acrylic acid and it has the excellent cohesional strength, good physical and chemistry stability. The carboxyl groups introduced by acrylic acid are potential functionality for the formation of hydrogen bonding with fillers such as silica, clays and halloysite nanotubes (HNTs) (Du, Guo, Lei, Liu, & Jia, 2008). In the present work, we attempt to fabricate CNs via acid hydrolysis of cotton linter with concentrated sulfuric acid, and then use the resulting CNs to reinforce XSBR matrix for preparation of a nanocomposite material with improved performance. As we all know, for preparation of a nanocomposite material with high mechanical properties, the major problem is the uniform dispersion of fillers in the matrix and a strong interfacial combination between the fillers and the matrix. In this case, the abundant hydroxyl groups on the surface of CNs make them possible to form strong hydrogen bonds with the carboxyl groups of XSBR. Considering that the nature of serious aggregation of CNs when they are dried, XSBR/CNs composites were prepared by mixing a water suspension of CNs with the water based XSBR latex directly. As expected, the CNs showed significant reinforcing effects on XSBR. The morphology, structure and properties of the resulting nanocomposites were investigated by scanning electron microscopy (SEM), dynamic mechanical analysis (DMA), rubber process analysis (RPA), thermal gravimetric analysis (TGA) and mechanical properties tests carefully.

2. Experimental and method

2.1. Materials

Cottonseed linter was supplied by Hubei Chemical Fiber Manufacture, China. Concentrated sulfuric acid (98%) was purchased from Sigma–Aldrich Corporation and used as received without further purification. Sulfur, zinc oxide, stearic acid, accelerators, and other additives were of industrial grade and used as-received. Carboxylate butadiene-styrene (XSBR) latex with 48% solids was obtained from Quanzhou Deli Chemical Co., Ltd. (DL659, Fujian, China), which is a random copolymer consisting of 33 wt% butadiene, 64 wt% styrene and 3 wt% of carboxylate functional monomer. The chemical structure of XSBR is shown as below.

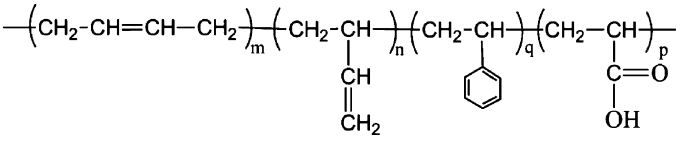

2.2. Preparation of cellulose nanocrystals

The cottonseed linter pulp (30 g) was cut into small pieces, and then mixed with sulfuric acid aqueous solution (250 mL, 64 wt%) under vigorous stirring at 60 °C for 2 h. Subsequently, the suspension was washed with water by successive centrifugation and dialyzed against deionized water until the pH of the suspension was neutral. Finally, a stable suspension with a solid content of 5.0 wt% was obtained through 10 min ultrasonic treatment, which then was stored in a refrigerator before use.

2.3. Preparation of XSBR/CNs composites

A desired content of CNs suspension was mixed with XSBR latex and stirred vigorously at room temperature for 30 min, and then the mixture was dried under reduced pressure at 60 °C until a constant weight was obtained. The compounding of XSBR/CNs with other ingredients was carried out on a two-roll mill. The rubber compound sheets were then compressed and vulcanized at 170 °C in an electrically heated hydraulic press for their optimal cure time (t_{90}) respectively, which was derived from curing curves. By changing the contents of CNs over the range of 0 phr, 3 phr, 5 phr, 10 phr and 15 phr, a series of nanocomposite sheets with a thickness of around 1 mm were prepared and coded as XSBR, XSBR-3N, XSBR-5N, XSBR-10N, and XSBR-15N respectively. In addition, the other components of the XSBR/CNs nanocomposites were fixed as follows (phr): XSBR 100, sulfur 1.5, zinc oxide 5, stearic acid 2, N-cyclohexylbenzothiazole-2-sulphenamide 1.5 phr, sulfenamide 2,2′-dibenzothiazole disulfide 0.5.

2.4. Curing characteristics

The curing curves at 170 °C were recorded in a M2000 Rheometer (Gotech Testing Machines Inc., Taiwan). The relative curing degree was represented by the variation between the maximal torque value (M_H) and the minimal torque value (M_L) of the curing curve.

2.5. Dynamic mechanical analysis (DMA)

The dynamic mechanical behaviors of the XSBR/CNs nanocomposites were determined by a dynamic mechanical analyzer (DMA242C NETZSCH; Germany) in tension mode. The temperature program was run from −100 to +150 °C using a heating ramp of 5 °C min^{-1} at a fixed frequency of 10 Hz. The samples were prepared as a cut strip with the size of 8 mm × 1 mm × 6 mm (length × thickness × width).

2.6. Morphological studies

EVO18 SEM (NEISS, Germany) was used to observe the phase morphology of XSBR/CNs composites. The cryogenically fractured surfaces of the specimens were sputter-coated with gold prior to analysis.

2.7. Crosslink density measurement

The apparent crosslink density was determined by equilibrium swelling experiments. To calculate the crosslink density, five weighed test pieces of rubber were immersed in toluene at about 23 °C for 72 h in sealed dark vials. Then, the samples were blotted with tissue paper to remove the excess of solvent and immediately weighed on an analytical balance. Finally, the samples were dried in a vacuum oven for 48 h at 60 °C until a constant weight was reached. The volume fraction of rubber swollen in the gel, V_r, which was used to represent the crosslink density of the samples, was determined by the following equation:

$$V_r = \frac{m_0\varphi(1-\alpha)\rho_r^{-1}}{m_0\varphi(1-\alpha)\rho_r^{-1} + (m_1 - m_2)\rho_s^{-1}} \quad (1)$$

where m_0 is the mass of the sample before swollen, m_1 and m_2 are the masses of the swelled sample before and after drying, respectively, φ is the mass fraction of rubber in the vulcanizates, α is the

mass loss of the vulcanizates after swollen, ρ_r and ρ_s are the rubber and toluene density ($\rho_s = 0.865\ g/cm^3$), respectively.

2.8. Thermal gravimetric analysis (TGA)

A thermogravimeter (TGA 209, NETZSCH, Germany) was used to measure the weight loss of the XSBR/CNs composites under nitrogen atmosphere. The samples were heated from ambient temperature up to 700 °C at a heating rate of 20 °C min^{-1}. Generally, approximately 10 mg of sample was used for each thermogravimetric analysis.

2.9. RPA2000 test

The experiments, including frequency sweeps and strain sweeps, were conducted by RPA2000 (Alpha technologies Co., UK). The cavity house was a biconical test chamber closed by the action of a pneumatic ram operated at a pressure. A slight excess of test material was needed to ensure the cavity house was full. Tests were thus made under pressurized conditions to make sure that porosity did not develop in the samples during the tests. The temperature was kept at 60 °C before the uncured samples were subjected into the cavity house for conducting the strain sweep (or frequency sweep). Subsequently, the temperature was raised to 170 °C to vulcanize the composites for their optimal cure time (t_{90}). After curing, the temperature was cooled down to 60 °C again, and the strain sweep (or frequency sweep) for vulcanizate was conducted. Strain sweeps were performed from 0.7 to 280% and the frequency were kept at 60 cpm (cycles per minute). Frequency sweeps were performed from 1 to 1000 cpm and the test strain was fixed at 1%.

2.10. Mechanical properties

The stress-strain properties were measured with dumbbell specimens (6 mm width in crosssection) according to ASTM D412. Tear strength was measured on un-nicked 90° angle test pieces according to ASTM D624. Tensile tests were carried out using a Computerized Tensile Strength Tester (UT-2080) produced by U-CAN Dynatex Inc. (Taiwan) with a crosshead speed of 500 mm/min. Shore A hardness was determined under the conditions given in ASTM-D2240.

3. Results and discussion

3.1. Morphological characterization of CNs prepared via acid hydrolysis

The CNs prepared from sulfuric acid hydrolysis of cottonseed linter was characterized by SEM with the result as shown in Fig. 1. As can be seen, the diameters of individual fibril aggregates are mainly found to be nanoscale, and most CNs size is less than 50 nm. The length of most of them is found to be less than 500 nm. This is in good agreement with the reported data for CNs produced from the same cellulosic material under similar conditions (Dufresne, 2008). However, it should be noted that a wide distribution of CNs size, especially the length, is inevitable owing to the diffusion-controlled nature of the acid hydrolysis.

3.2. Vulcanization process of XSBR/CNs compounds

The cure-curves and curing characteristics of XSBR containing different CNs content are shown in Fig. 2. It is clear that the addition of CNs leads to an increase in M_H of the XSBR/CNs composites. The ultimate torque value of XSBR-15N is increased nearly 10 dNm compared with that of XSBR. The XSBR molecular can be adsorbed

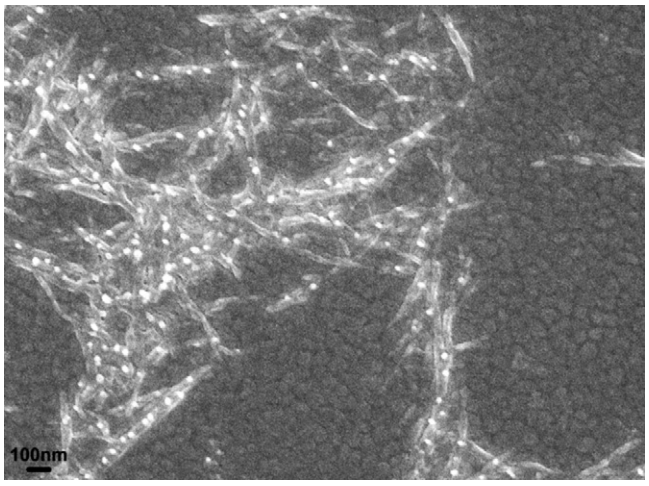

Fig. 1. The SEM image of CNs.

onto the surface of CNs via physical adsorption or hydrogen bonding effect, which could introduce extra crosslinks in the XSBR/CNs composites. M_L of XSBR/CNs composites are nearly unchanged with increasing CN content, but slightly lower than that without CNs. These results prove that CNs can improve the crosslink density of XSBR and possibly lead to an enhanced mechanical property. As we know, the t_{10} indicates the pre-vulcanization characteristics during processing. If the t_{10} is too low, the viscosity of the rubber compound will increase too fast, so that the rubber composites can not take the shape of the designed products. The t_{10} of XSBR/CNs compounds almost unchanged with the increase of CNs, implying that CNs do not negatively influence the pre-vulcanization processes of XSBR.

3.3. RPA 2000 analysis of the XSBR/CNs composites

Fig. 3a shows a plot of storage modulus (G') versus the strain of uncured composites. The modulus of XSBR/CNs composites increase gradually with an increase of CNs content. The G' of XSBR-3N is very close to that of pure XSBR, which indicates that the filler–filler network is not formed at 3 phr CNs. When the CNs content reaches 5 phr CNs, the G' is obviously higher than that of XSBR. The plot curves exhibit a typical nonlinear relationship with increasing strain, which is generally called as 'Payne effect' (Payne, 1965; Payne & Whitaker, 1971). It was also observed that the 'Payne

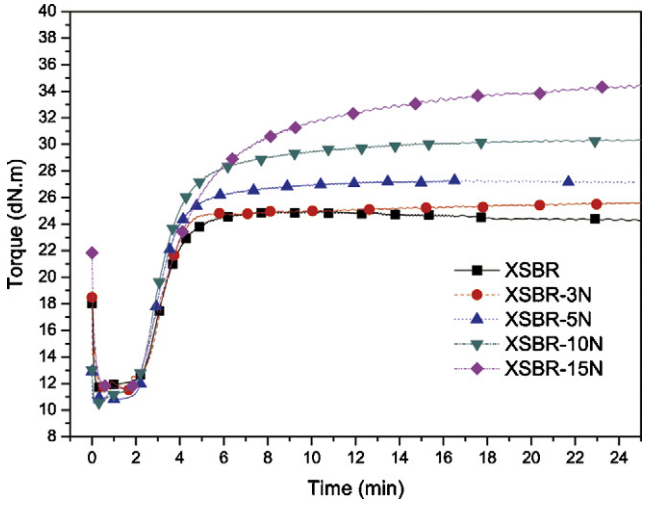

Fig. 2. Curing behavior of XSBR/CNs composites.

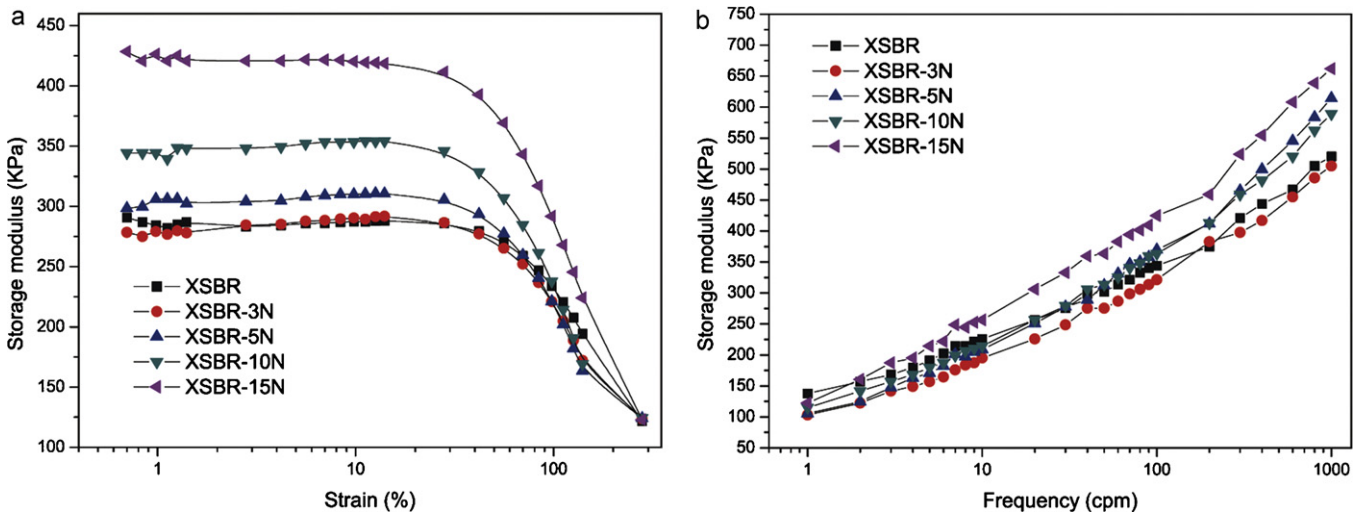

Fig. 3. G'–strain curves (a) and G'–frequency curves (b) of the uncured XSBR/CNs composites.

effect' is enhanced with the increasing CNs content. Even at 15 phr CNs, the linear viscoelastic region (LVE) still reveals that the G' is independent on shear strain at a large strain range. When the strain exceeds about 10%, the storage modulus shows a significant drop with the growth of the strain, which is a typical feature of structure breakdown. This phenomenon demonstrates that a developed and strong three-dimensional filler–filler network was formed even at a small load of 5 phr CNs. Payne effect is regarded as a result of breakage and reforming of physical bonds between the filler aggregates. The stronger the rebuilt ability of the filler–filler networks was, the higher the strain amplitudes was used to break down the networks (Chen, Xu, & Wang, 2012). The strong three-dimensional filler–filler network formed in uncured compounds should be attributed to the higher aspect ratio of CNs and the strong attraction between hydroxyl group of CNs. Fig. 3b shows the plot of G' versus the frequency of uncured composites. The increase in G' with increasing frequency can be assigned to the decrease in time available for molecular relaxation at high frequency. In addition, with the higher loading of CNs, the larger value of G' can be observed at high frequency. This result also proves the formation of three-dimensional network of CNs when the CNs load is higher than 5 phr.

3.4. Dynamic mechanical performance of the XSBR/CNs composites

Dynamic mechanical analysis (DMA) was carried out to identify the dynamic response of XSBR/CNs composites. The dependency of storage modulus (E') as a function of temperature was given in Fig. 4. All samples show a steep decrease of E' value at the temperature range between 25 and 45 °C, followed by a rubbery plateau (Fig. 4a). Increasing the amount of CNs, a successive increase of the values of E' can be observed. For example, the storage modulus at −100 °C increases from ~2700 MPa to 4200 MPa with the addition of CNs from 0 to 15 phr in the XSBR matrix. The enhancement in modulus below glass transition temperature is a good evidence for the strong reinforcing tendency of CNs in the XSBR matrix. A sufficiently strong filler–filler interactions as well as the compatibility between CNs and XSBR are playing a major role in the case.

Fig. 4b shows the variation of tan δ as a function of temperature for composites with various concentrations of CNs. tan δ exhibits a maximum value at a temperature around 50 °C, which can be altered by changing the CNs content. Generally, the glass transition temperature (T_g) of polymer can be shifted to higher temperature after incorporation of nano-fillers, because nano-fillers hinder the segmental motion of polymer chain segments. However, this disciplinary experience does not take effect in our study. As shown in Fig. 4b, T_g is shifted from 48.45 °C to 50.64 °C with the addition of only 3 phr CNs in the XSBR matrix. However, T_g is decreased from 50.64 to 46.28 °C with increasing CNs to 15 phr. It is well understood that the strong polarity can improve T_g of polymer matrix. The hydroxyl groups on the CNs surface can easily form hydrogen bonds with the carboxyl groups in XSBR molecular. This may act as an internal plasticization which results in the shifting of T_g to a lower temperature with increasing CNs. However, further study is still needed to investigate the essential reason for this particular phenomenon. No significant broadening of the tan δ peak is observed in Fig. 4b. Finally, the intensity of the relaxation process decreases with increasing amount of CNs, and it is ascribed to the decrease of matrix material amount, which is responsible for damping properties.

3.5. Morphology analysis of XSBR/CNs composite

Fig. 5 illustrates the SEM images of cryogenically fractured surfaces of the unfilled XSBR matrix and XSBR/CNs composite containing 5, 10, and 15 phr CNs, respectively. Compared to the micrograph of unfilled XSBR, the morphology of the CNs in the XSBR matrix can be easily identified. The CNs appear as white dots and their concentration on the fracture surface of the composites increase directly with an increase of the filler loading. A uniform distribution of CNs in the XSBR matrix can be observed in all of the XSBR/CNs composites, though some CNs aggregates still exist at a higher load of CNs. However, it is obvious that those CNs dots or aggregates are partial embedded in XSBR matrix, demonstrating the good compatibility between the fillers and matrix. Furthermore, the SEM images showed no gaps, no voids and no pull out cracks on the surface, indicative of the excellent interfacial adhesion between the CNs and XSBR matrix. The fantastic compatibility and interfacial adhesion between XSBR and CNs can be ascribed to the strong attraction between carboxyl groups and hydroxyl groups. Thus, although the presence of hydroxyl groups on the surface of CNs makes it hydrophilic and thus increases the surface energy, the XSBR matrix has a considerable cohesive energy and a strong polar nature due to the carboxyl groups. Such uniform distribution of the fillers in the matrix is anticipated to play an important role in the improvement of the mechanical performance of the resulting XSBR/CNs composites.

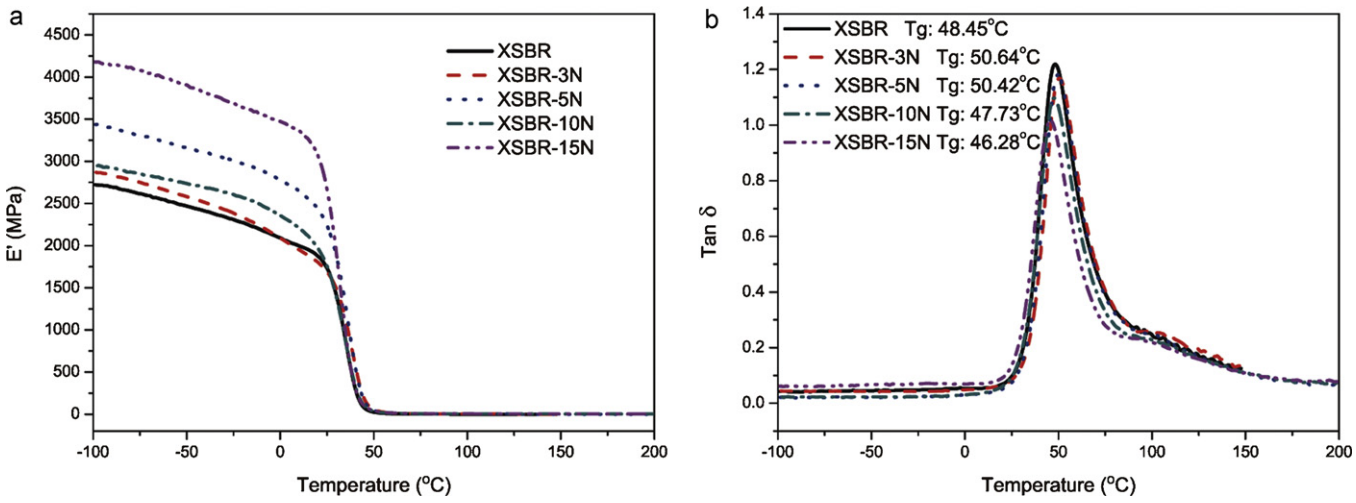

Fig. 4. E'–T curves (a) and tan δ–T curves (b) of cured XSBR/CNs composites.

3.6. Apparent crosslink densities of XSBR/CNs composites

Apparent crosslink density of XSBR/CNs composites was given in Fig. 6. With an increasing amount of CNs, the crosslink density shows an apparent increase for XSBR/CNs composites, except the XSBR-3N. These results are in good accordance with the above-mentioned conclusion that the M_H increased with the addition of CNs. The possible hydrogen bonding formed between hydroxyl groups of CNs and carboxyl groups of XSBR molecular will possibly function as crosslinking points which increase crosslink density. Furthermore, the adsorption of rubber molecular to the surface of CNs also yields the improved apparent crosslink density,

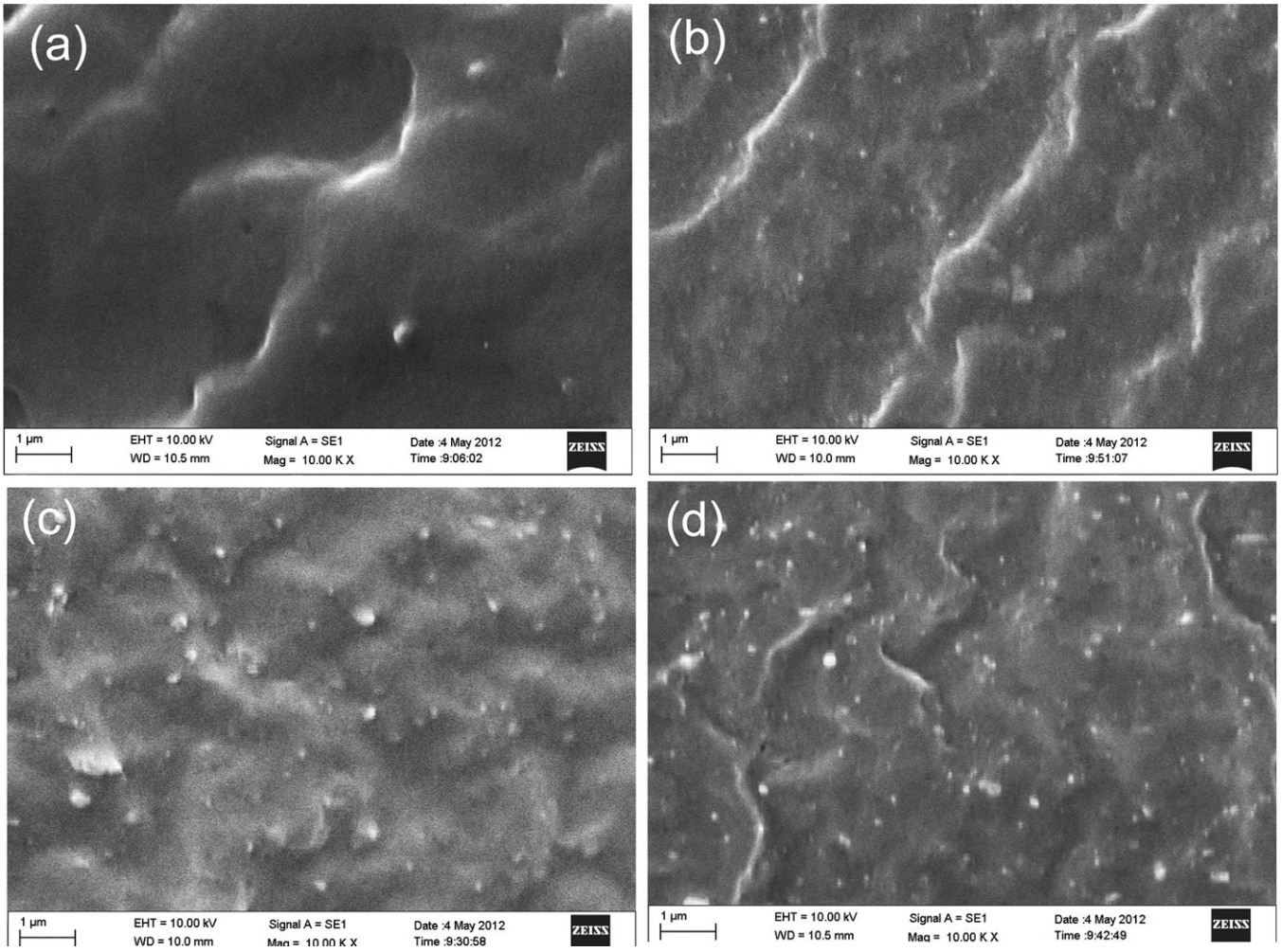

Fig. 5. SEM images for the cryogenically fractured surfaces of XSBR/CNs composites: (a) XSBR; (b) XSBR-5N; (c) XSBR-10N; (d) XSBR-15N.

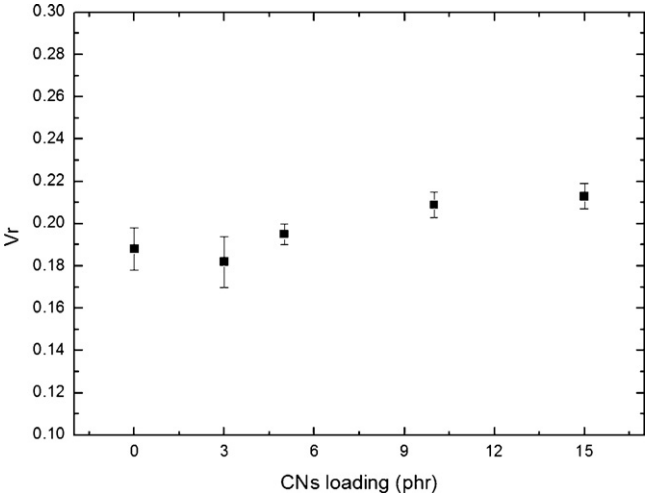

Fig. 6. Apparent crosslink densities of XSBR/CNs composites.

which is well understood in a nano-filler reinforced rubber system.

3.7. Mechanical properties

Previous studies showed that strong interaction by hydrogen bonding between hydroxyl groups on cellulose and the functionalized host matrix increased the polymer strength. Similar phenomenon was also observed in this study. The mechanical properties of the XSBR/CNs composites are shown in Fig. 7. The tensile strength (Fig. 7a), the tear strength (Fig. 7c) and shore A hardness (Fig. 7d) of the XSBR/CNs composites increase with increasing CNs in the matrix. The tensile strength and tear strength increase from 16.9 to 24.1 MPa and from 43.5 to 65.2 MPa, respectively, with increasing CNs content from 0 to 15 phr. This reveals that CNs indeed show a good reinforcement on the XSBR. The improved mechanical properties are related to the good uniform distribution of CNs in the XSBR matrix and the good interfacial interaction between the CNs and the XSBR matrix. And these results are also in accordance with the crosslinking density analysis. Compared with Du's (Du et al., 2008) report that the tensile strength of XSBR increased only about 5.3 MPa with increasing HNTs content from 0 to 30 phr, CNs has an advantage in reinforcing XSBR at a lower content. The elongation at break also is improved by addition of CNs, as shown in Fig. 7b.

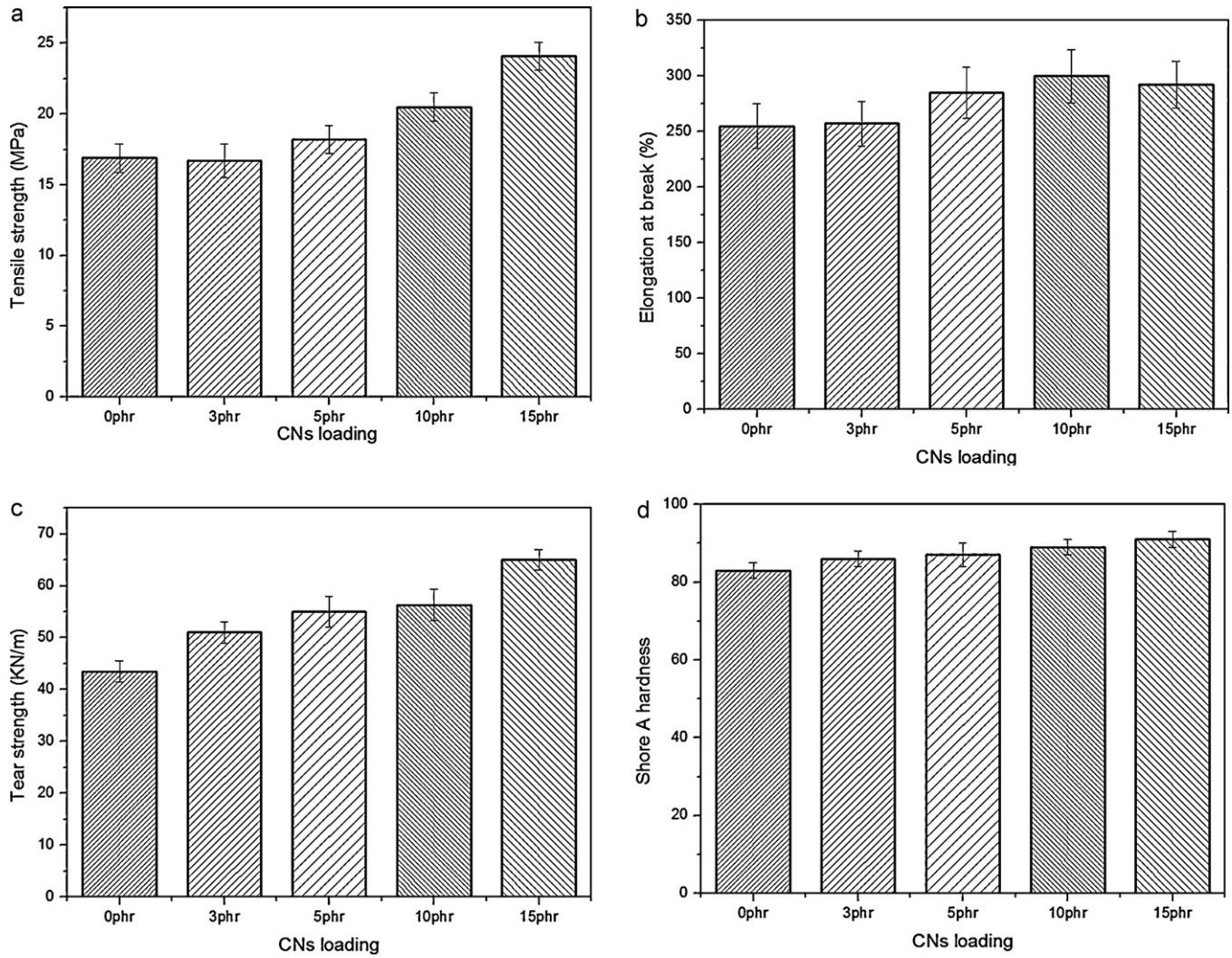

Fig. 7. Mechanical properties of the XSBR/CNs composites: (a) tensile strength; (b) elongation at break; (c) tear strength; (d) shore A hardness.

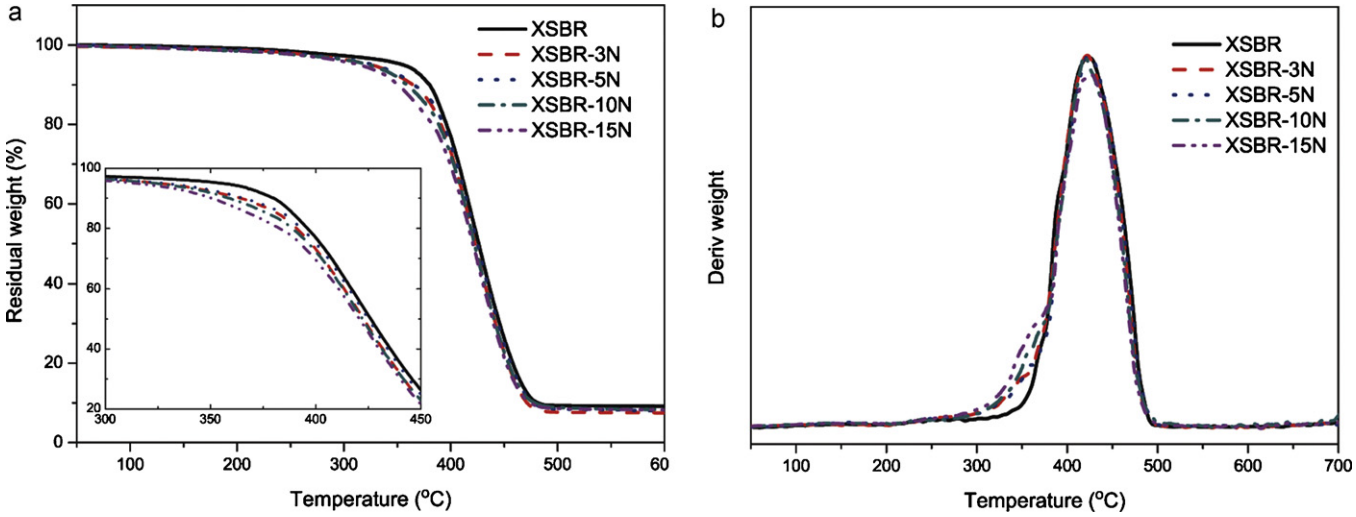

Fig. 8. TG curves (a) and DTG curves (b) of XSBR/CNs composites.

3.8. Thermal stability analysis

Fig. 8a and b show the TG and DTG curves of XSBR/CNs composites with various loading levels of CNs. Generally, the degradation of CNs possessing sulfate groups that arised from hydrolysis with sulfuric acid occurs between 200 and 300 °C due to its depolymerization, dehydration, and decomposition of glycosyl units followed by the formation of a char. However, no separate degradation stage of the CNs can be found in any TG curves of the XSBR/CNs composites regardless of the CNs loading level, which indicates that CNs have been completely covered by the XSBR molecules through the possible hydrogen bonding between CNs and XSBR. Meanwhile, the temperature of maximum weight loss rate of all the samples was nearly unchanged, while both the temperature at 5% weight loss and residual mass were gradually decreased with the increase of CNs. These results may be originated from the decomposition of CNs before XSBR. Nevertheless, the maximum weight loss rate of the composites is not affected apparently, which may be attributed to a strong rigid network of CNs formed in the XSBR matrix via hydrogen bonding.

4. Conclusion

Carboxylated styrene-butadiene rubber (XSBR)/cellulose nanocrystals (CNs) composites were successful prepared by mixing water suspension of CNs and XSBR latex. Inclusion of higher CNs content shifted the glass transition temperature of XSBR/CNs composites to a lower temperature. The good compatibility led to a good distribution uniformity of the CNs in the XSBR matrix. The good interfacial adhesion between CNs and the rubber matrix and the improved crosslink density were correlated to the considerable reinforcing effects of CNs. The CNs decreased the temperature at 5% weight loss of the XSBR/CNs composites, but not apparently affected the maximum weight loss rate.

Acknowledgements

This work was financially supported by the grants from Program for New Century Excellent Talents in University (NCET-11-0148), Specialized Research Fund for the Doctoral Program of Higher Education (20110172120002) and the State Key Laboratory of Pulp and Paper Engineering of China (Grant No. 201101).

References

Araki, J., Wada, M., Kuga, S., & Okano, T. (1998). Flow properties of microcrystalline cellulose suspension prepared by acid treatment of native cellulose. *Colloids and Surfaces A*, *142*, 75–82.
Azizi Samir, M. A. S., Alloin, F., & Dufresne, A. (2005). Review of recent research into cellulosic whiskers, their properties and their application in nanocomposite field. *Biomacromolecules*, *6*, 612–626.
Bai, W., & Li, K. C. (2009). Partial replacement of silica with microcrystalline cellulose in rubber composites. *Composites Part A*, *40*, 1597–1605.
Beck-Candanedo, S., Roman, M., & Gray, D. G. (2005). Effect of reaction conditions on the properties and behavior of wood cellulose nanocrystal suspensions. *Biomacromolecules*, *6*, 1048–1054.
Bendahou, A., Kaddami, H., & Dufresne, A. (2010). Investigation on the effect of cellulosic nanoparticles' morphology on the properties of natural rubber based nanocomposites. *European Polymer Journal*, *46*, 609–620.
Bokobza, L., Rahmani, M., Belin, C., Bruneel, J. L., & El Bounia, N. E. (2008). Blends of carbon blacks and multiwall carbon nanotubes as reinforcing fillers for hydrocarbon rubbers. *Journal of Polymer Science Part B: Polymer Physics*, *46*, 1939–1951.
Cao, X. D., Habibi, Y., & Lucia, L. A. (2009). One-pot polymerization, surface grafting, and processing of waterborne polyurethane-cellulose nanocrystal nanocomposites. *Journal of Materials Chemistry*, *19*, 7137–7145.
Cao, X. D., Habibi, Y., Magalhaes, W. L. E., Rojas, O. J., & Lucia, L. A. (2011). Cellulose nanocrystals-based nanocomposites: Fruits of a novel biomass research and teaching platform. *Current Science*, *100*, 1172–1176.
Chen, Y., Liu, C. H., Chang, P. R., Cao, X. D., & Anderson, D. P. (2009). Bionanocomposites based on pea starch and cellulose nanowhiskers hydrolyzed from pea hull fibre: Effect of hydrolysis time. *Carbohydrate Polymers*, *76*, 607–615.
Chen, Y. K., Xu, C. H., & Wang, Y. P. (2012). Viscoelasticity behaviors of lightly cured natural rubber/zinc dimethacrylate composites. *Polymer Composites*, *33*, 967–975.
Du, M. L., Guo, B. C., Lei, Y. D., Liu, M. X., & Jia, D. M. (2008). Carboxylated butadiene-styrene rubber/halloysite nanotube nanocomposites: Interfacial interaction and performance. *Polymer*, *49*, 4871–4876.
Dufresne, A. (2008). Polysaccharide nano crystal reinforced nanocomposites. *Canadian Journal of Chemistry*, *86*, 484–494.
Dupres, S., Long, D. R., Albouy, P. A., & Sotta, P. (2009). Local deformation in carbon black-filled polyisoprene rubbers studied by NMR and X-ray diffraction. *Macromolecules*, *42*, 2634–2644.
Favier, F., Chanzy, H., & Cavaille, J. Y. (1995). Polymer nanocomposites reinforced by cellulose whiskers. *Macromolecules*, *28*, 6365–6367.
Fengel, D., & Wegner, G. (1984). *Wood: Chemistry, ultrastructure, reactions*. New York: Walter de Gruyter.
Grunert, M., & Winter, W. T. (2002). Nanocomposites of cellulose acetate butyrate reinforced with cellulose nanocrystals. *Journal of Polymers and the Environment*, *10*, 27–30.
Hanley, S. J., Giasson, J., Revol, J. F., & Gray, D. G. (1992). Atomic force microscopy of cellulose microfibrils: Comparison with transmission electron microscopy. *Polymer*, *33*, 4639–4642.
Helbert, W., Cavaille, J. Y., & Dufresne, A. (1996). Thermoplastic nanocomposites filled with wheat straw cellulose whiskers, Part I: Processing and mechanical behavior. *Polymer Composites*, *17*, 604–611.
Kim, B., Seo, J., & Jeong, H. (2003). Morphology and properties of waterborne polyurethane/clay nanocomposites. *European Polymer Journal*, *39*, 85–91.
Kuan, H., Ma, C., Chuang, W., & Su, H. (2005). Hydrogen bonding, mechanical properties, and surface morphology of clay/waterborne polyurethane nanocomposites. *Journal of Polymer Science Part B: Polymer Physics*, *43*, 1–12.

Kuan, H., Ma, C., Chang, W., Yuen, S., Wu, H., & Lee, T. (2005). Synthesis, thermal, mechanical and rheological properties of multiwall carbon nanotube/waterborne polyurethane nanocomposite. *Composites Science and Technology*, *65*, 1703–1710.

Kwon, J., & Kim, H. (2005). Comparison of the properties of waterborne polyurethane/multiwalled carbon nanotube and acid-treated multiwalled carbon nanotube composites prepared by in situ polymerization. *Journal of Polymer Science Part A: Polymer Chemistry*, *43*, 3973–3985.

Lee, H., Hwang, J., & Liu, H. (2006). Effects of ionic interactions between clay and waterborne polyurethanes on the structure and physical properties of their nanocomposite dispersions. *Journal of Polymer Science Part A: Polymer Chemistry*, *44*, 5801–5807.

Lee, H., & Lin, L. (2006). Waterborne polyurethane/clay nanocomposites: Novel effects of the clay and its interlayer ions on the morphology and physical and electrical properties. *Macromolecules*, *39*, 6133–6141.

Lu, Y., Weng, L., & Cao, X. (2006). Morphological, thermal and mechanical properties of ramie crystallites-reinforced plasticized starch biocomposites. *Carbohydrate Polymers*, *63*, 198–204.

Magalhaes, W. L. E., Cao, X. D., & Lucia, L. A. (2009). Cellulose nanocrystals/cellulose core-in-shell nanocomposite assemblies. *Langmuir*, *25*, 13250–13257.

Mathew, A. P., & Dufresne, A. (2002). Morphological investigation of nanocomposites from sorbitol plasticized starch and tunicin whiskers. *Biomacromolecules*, *3*, 609–617.

Payne, A. R. (1965). A note on the conductivity and modulus of carbon black-loaded rubbers. *Journal of Applied Polymer Science*, *9*, 1073–1082.

Payne, A. R., & Whitaker, R. E. (1971). Low strain dynamic properties of filled rubber. *Rubber. Rubber Chemistry and Technology*, *44*, 440–478.

Podsiadlo, P., Choi, S., Shim, B., Lee, J., Cussihy, M., & Kotov, N. (2005). Molecularly engineered nanocomposites: Layer-by-layer assembly of cellulose nanocrystals. *Biomacromolecules*, *6*, 2914–2918.

Revol, J. F. (1982). On the cross-sectional shape of cellulose crystallites in *Valonia ventricosa*. *Carbohydrate Polymers*, *2*, 123–134.

Sturcova, A., Davies, G. R., & Eichhorn, S. J. (2005). Elastic modulus and stress-transfer properties of tunicate cellulose whiskers. *Biomacromolecules*, *6*, 1055–1061.

Terech, P., Chazeau, L., & Cavaille, J. Y. (1999). A small-angle scattering study of cellulose whiskers in aqueous suspensions. *Macromolecules*, *32*, 1872–1875.

Thongsang, S., Sombatsompop, N., & Ansarifar, A. (2008). Effect of fly ash silica and precipitated silica fillers on the viscosity, cure, and viscoelastic properties of natural rubber. *Polymers for Advanced Technologies*, *19*, 1296–1304.

Tokoh, C., Takabe, K., Fujita, M., & Saiki, H. (1998). Cellulose synthesized by *Acetobacter xylinum* in the presence of acetyl glucomannan. *Cellulose*, *5*, 249–261.

Wu, Y. P., Qi, Q., Liang, G. H., & Zhang, L. Q. (2006). A strategy to prepare high performance starch/rubber composites: In situ modification during latex compounding process. *Carbohydrate Polymers*, *65*, 109–113.

Xu, S. H., Gu, J., Luo, Y., & Jia, D. (2012). Effects of partial replacement of silica with surface modified nanocrystalline cellulose on properties of natural rubber nanocomposites. *Express Polymer Letters*, *6*, 14–25.